Ordered Mesoporous Particles in Titania Films with Hierarchical Structure as Scattering Layers in Dye Sensitized Solar Cells

Yuli Xiong,[a] *Daping He,*[b] *Yun Jin,*[a] *Petra J. Cameron* [a] and *Karen J. Edler**[a]

[a] Department of Chemistry, University of Bath, Claverton Down, Bath BA2 7AY, UK.

[b] Department of Chemistry, University of Science and Technology of China , Hefei, Anhui 230026, China.

ABSTRACT: This work aimed to understand the relationship between the physical properties of scattering particle layers in Dye Sensitized Solar Cells (DSSC) to their performance, to assist optimization of this component of the DSSC. Highly ordered anatase 2D-hexagonal mesoporous titania (meso-TiO_2) nanoparticles with a high surface area and large pore size were fabricated. Meso-TiO_2 was used as scattering particles and mixed with titania nanocrystallites at weight proportions ranging from 0 to 100%. Films made from the composites were used as scattering layers in DSSC. The influence of meso-TiO_2 proportion on the structure, morphology and optical properties of the films were investigated. The results show that the films became more porous, with a larger surface roughness, had higher surface areas and greater light scattering effects when meso-TiO_2 was incorporated. The performance of these scattering layers in relatively large, 1cm^2 area, DSSC was studied to link cell performance to the detailed physical properties of the meso-TiO_2/nanoparticle films. The optimum composition of scattering layers was obtained by mixing 50 wt.% meso-TiO_2 with titania nanoparticles.

KEYWORDS: anatase membrane, mesoporous, nanowire, solution interface, solar cell.

Introduction

Dye sensitized solar cells (DSSC) are one of the promising clean energy harvesting devices and have been the subject of intensive studies currently achieving efficiencies over 12 %.[1] By harvesting photons, dye molecules, absorbed on a titania photoelectrode surface, generate electrons that are injected into and diffuse through the titania network, while the charged dye molecules are regenerated by a redox couple (typically iodide/triiodide) in electrolyte solution. The iodide is reduced at a platinum electrode by the electrons that have travelled from the external circuit.[2] It is obvious that many factors can affect the performance of DSSC but the structural and physical properties of the titania electrode are among the most important.[3-4] Compared with using only nanocrystalline TiO_2 particle films, it has been demonstrated that the photocurrent density can be improved by mixing submicron-sized particles with nanocrystalline TiO_2 in mono and/or bilayer structures composed of a light scattering layer and a nanocrystalline semitransparent TiO_2 layer.[5] The confinement of incident light by the light scattering particles causes more photons to be harvested.[5-6] Since the particle size, surface area and position of the scattering particles plays an important role in light scattering and dye uptake of photoelectrode,[7-8] a suitable combination of nanoparticles and scattering particles is essential to improve the cell performance.

Recently, mesoporous TiO_2 (meso-TiO_2) particle has been synthesized for DSSC in micron/submicron particle geometries with hierarchical structures, such as titania aggregates, [9-10] beads,[11-12] spheres,[13-14] and inverse opal structures.[15] These porous structures are composed of primary nano-crystallites that cluster together to form larger secondary particles, thereby functioning as light scatterers without sacrificing the internal surface area needed for effective dye–uptake when applying them in DSSC. These films were applied as a photoelectrode film

directly or as the scattering layer and showed an improved cell performance. However, the combination of nanocrystalline TiO_2 particle and submicron titania aggregates as a scattering layer has not so far been discussed. The extra steps required to initially synthesise a larger porous TiO_2 particle will contribute to a higher cost of these materials, so if the amount of this material can be optimised, in combination with cheaper nanocrystalline TiO_2 building blocks, the benefits of the larger particle incorporation can be realised while the cost of the final device will be reduced.

Here, we propose using ordered 2D-hexagonal meso-TiO_2 aggregates and nanocrystalline TiO_2 particle composite films as the scattering layer of the DSSC. The weight ratio of the aggregates and nanocrystalline particles was adjusted to obtain an optimal mixture. Meso-TiO_2 particles have large internal pores and an ultrahigh surface area to increase dye loading and the open spaces between large aggregates help ensure efficient electrolyte diffusion.[9, 11, 16] Work has also suggested that surfactant templated mesoporous titanias have good intra-grain connectivity between crystallites in the walls between pores that promotes facile charge transport[10]. Ordered mesoporosity will ensure consistency of pore dimensions and wall structures throughout the particle to maximize these advantages. A bilayer photoelectrode was used in a DSSC with the underlying layer made from a commercial titania paste and the scattering layer from meso-TiO_2 aggregates, titania nanoparticles (P25) or their mixtures. The influence of film structure, morphology, optical properties and cell performance were investigated, in films prepared by adding meso-TiO_2 into a paste containing P25 nanoparticles, with weight proportion ranging from 0 to 100%. We note that the cells were not optimised for the highest efficiencies as our emphasis was on studying the differences introduced by a mesostructured scattering layer. The results showed an improved photovoltaic performance of DSSC with meso-TiO_2 and the best cell

was obtained by incorporating 50 wt.% meso-TiO_2. Further optimization of these devices for higher efficiency was beyond the scope of this work.

Experimental

Synthesis of ordered mesoporous titania and pastes

All chemicals were used as supplied. Ordered mesoporous titania was prepared from titanium tetraisoproxide (TiPr, Acros, ≥ 98%) as a precursor, Pluronic P-123 (Sigmal-Aldrich, MW ~5800) as a surfactant template and a mixture of HCl and H_2SO_4 as the acidic catalyst.[17] 1.0 g of P-123 was dissolved in 40 ml ethanol (AR, Sigmal-Aldrich), to which 1ml HCl (Fisher, 32%) and 0.2 ml H_2SO_4 (Fisher, 98%) were added. The solution was placed into a bottle sealed with a cap and stirred vigorously for 3 hrs at room temperature. 2.9 ml TiPr was added dropwise at room temperature followed by vigorous stirring for 20 hrs at 40 °C. The solution was poured into petri dishes and evaporated at 40 °C in air under relative humidity of 55 % for 6 days. The resulting membranes were crushed into powder and calcined in air at 350 °C for 3 hrs, followed by a further 3 hrs at 450 °C, the temperature was ramped at 1°C/min.

The synthesized templated titania (meso-TiO_2) powders were mixed with commercial P25 nanoparticles (particle size ~21 nm, ≥ 99.5%, Sigma Aldrich) at different weight ratios. The mixtures were ground thoroughly before use and were named meso-X (X= 0, 25, 50, 75 or 100) where X represents the weight percentage of the meso-TiO_2 in the mixture.

Titania paste was prepared by mixing titania powder with ethyl cellulose (48% in ethoxy, viscosity 5-15 cp, Sigma Aldrich; 48% in ethoxy, viscosity 35-50 cp, Sigma Aldrich) as a binder and terpineol (≥ 99.5%, Sigma Aldrich) as the solvent. The final weight ratio of titania, ethyl

cellulose and terpineol was 3:2:10. The synthesis was done according to the procedure described in Scheme 1.

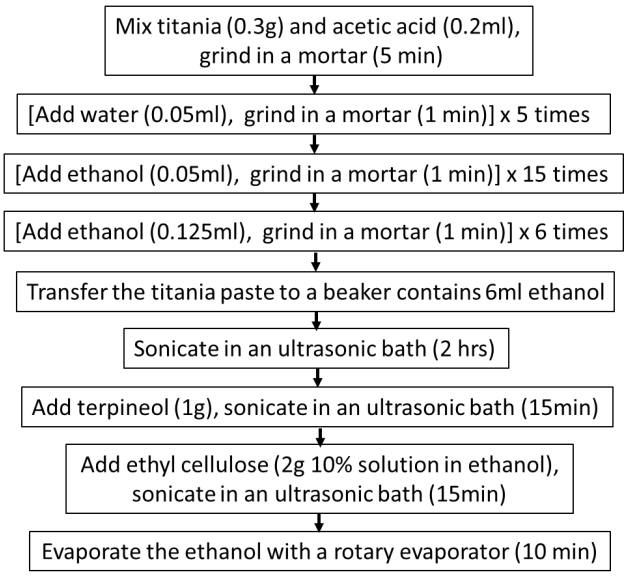

Scheme1 Fabrication method for TiO_2 pastes.

FTO glass (Hartford, TEC 15) was cleaned with Milli-Q water (18.2 MΩcm resistance), DECON 90 (Decon), Acetone (Fisher, LRG) and ethanol (Fisher, ARG). To prepare the photoanode, a blocking layer of TiO_2 was applied to the conducting side of the glass by spray pyrolysis on a hot plate at 400 °C using a solution of 0.2 mol/dm^3 titanium diisopropoxide bis(acetylacetonate) (Aldrich) in isopropanol. A bilayer nanocrystalline TiO_2 photoelectrode was then prepared. The first layer of nanocrystalline TiO_2 was deposited onto the FTO glass (7.5×2.5 cm^2) on top of the blocking layer, using a commercial paste (Ti-Nanoxide T, Solaronix) and the doctor blade method. 'Magic tape' (Scotch) was used to mark out a 1 cm wide strip on the glass and control the film thickness. The slide containing the first layer was then placed on a hotplate for 30 min at 100 °C. To minimize the effects of the first layer on the cells' performance, the FTO glass slide with a single Ti-Nanoxide layer was cut into 5 small pieces (1.5×2.5cm^2). Then the second layer was doctor bladed on top of each piece using one of five different home-made pastes. The

bilayer photoelectrodes were calcined. They were first heated to 130 ºC with a ramp speed of 2.5 ºC/min and held at 130 ºC for 15 min; then heated to 300 ºC at 6 ºC/min and held for 15 min, and finally to 450 ºC at 3 ºC/min and held for 30 min.

Device fabrication

After calcination, when films had cooled to 80 ºC, they were soaked in a solution of 0.3 mmol/dm^3 N719 dye (Dyesol, B2) in t-butanol (Sigma-Aldrich, 99.7%)/acetonitrile (Fisher, HPLC) solvent (volume ratio of 1:1) for 20 hrs at room temperature in blacked out containers. The dye-coated TiO_2 films were washed with t-butanol/acetonitrile, dried and then assembled with a Pt-coated counter electrode prepared by thermal decomposition of 5 mmol/dm^3 H_2PtCl_6 ($\geq$ 99.995 %, Sigma-Aldrich) solution in isopropanol which was spread onto an FTO glass slide at 390 ºC for 15 min. The two active electrodes were separated with a 25 μm thick Surlyn (Solaronix, SX1170-25PF) hot-melt gasket and sealed by heating. The internal space was filled with a liquid electrolyte using a vacuum backfilling system. A hole to inject the electrolyte was pre-drilled through the counter electrode and sealed after filling, with a Surlyn sheet and a thin glass cover slip by heating. The electrolyte used for fabrication of the device consists of 0.03 mol/dm^3 I_2 ($\geq$ 99.999%, Sigma Aldrich), 0.6 mol/dm^3 3-propyl-1-methylimidazolium iodide ($\geq$ 99%, Merck), and 0.1 mol/dm^3 guanidine thiocyanate ($\geq$ 99.0 %, Fluka) and 0.5 mol/dm^3 tert-butylpyridine ($\geq$ 99.0 %, Sigma Aldrich) in a mixture of acetonitrile (HPLC, Fisher) and valeronitrile ($\geq$ 99.5%, Sigma Aldrich) (volume ratio of 85:15). The resultant cells with active area of 1cm^2 were stored in the dark for 24 hrs prior to the measurement. Five sets of Meso-X solar cells were prepared and typical results are shown in this work.

Characterization

TGA was carried out to characterize the as-prepared meso-TiO_2 powders using a Perkin Elmer TGA 7 thermogravimetric analyser. SAXS (Anton PaarSAXSess using CuKα radiation from a PANalytical PW3830 generator) was used to check the mesostructure of as-prepared and calcined meso-TiO_2 powders. TEM images and diffraction pattern of calcined meso-TiO_2 were measured using a JEOL 1200 EX. Wide-angle powder XRD was used to examine the crystal structure using a Bruker D8 powder diffractometer with CuKα radiation. N_2 adsorption/desorption isotherms were taken using a BELSORP-mini II after degassing at 150 ºC for 4 hrs.

The morphology of the meso-X (X=0, 25, 50, 75 or 100) films was examined by SEM (JEOL JSM6480LV) and AFM (Nanosurf EasyScan 2 Flex). Cross-sectional images were also measured by SEM to estimate film thickness. Reflectance spectra were recorded using a UV-VIS-NIR from Ocean Optics. To investigate the crystal structure and N_2 adsorption/desorption isotherms of the P25/meso-TiO_2 mixtures in the photoanode films, films were doctor-bladed onto glass without the Ti-Nanoxide underlayer and calcined using the procedure described above, then scratched from the substrates. Their crystal structure was examined by wide-angle powder XRD and N_2 adsorption/desorption isotherms were taken after degassing at 150 ºC for 4 hrs.

After calcination the photoelectrode was immersed in 0.3 mmol/dm^3 dye N719 solution for 20 hrs, washed with t-butanol/acetonitrile solvent and dried completely. Adsorbed dye molecules were desorbed using 0.1 mol/dm^3 KOH aqueous solution. Quantification of the amount of adsorbed dye was carried out using an UV/Vis spectrometer (Varian, Cary 50 Probe).

IV curves were measured using a TS Space Systems solar simulator equipped with a 200W lamp and AM 1.5 filter, and a Keithley model 2601A digital source meter. They were calibrated with a

Si solar cell (Fraunhofer ISE, RS-OD-4) and tested under 1 sun illumination. The testing system was computer-controlled via a USB interface, using home written software. For IPCE measurements, a 150 W Xe lamp (Bentham 1L7S light source) was used as the light source to generate a monochromatic beam. Calibration was performed using a standard silicon photodiode (Thorlabs10102835).

Results and Discussion

The TGA curve of the as-prepared uncalcined meso-TiO_2 is shown in Figure S1 (supporting information). Weight loss below 130 °C was due to the evaporation of volatile species. The combustion of the P123 template occurs in the range between 130 to 300 °C. Above 300 °C, a small mass loss occurred due to the continuous removal of residual organic and sintering of TiO_2 particles.[18] After calcination, the meso-TiO_2 form aggregates with diameters in the range from 600 nm to several micrometers (Figure 1), which therefore can serve as scattering particles in a photoelectrode.

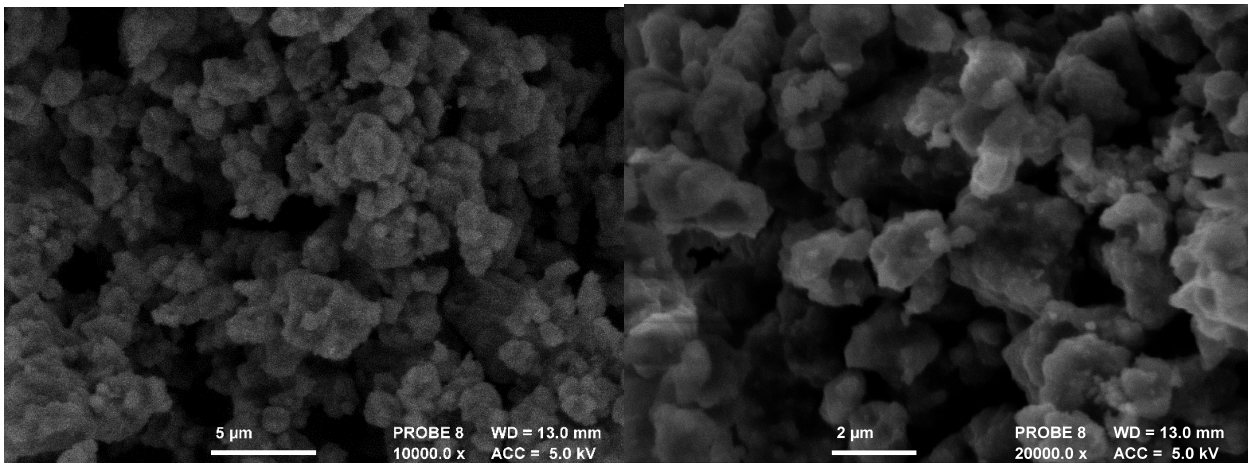

Figure 1 SEM images of calcined meso-TiO_2 at different magnifications.

Figure 2 (left) shows the SAXS patterns of the meso-TiO_2 material before and after calcination. Both patterns display similar shapes with four diffraction peaks arising from their ordered mesoscale structure. A clear shift of the diffraction peaks to a higher q was observed suggesting shrinkage of the titania network after removal of the template.[19-20] The peaks in the pattern for the calcined sample at q values of 0.59, 1.02, 1.18 and 1.56 nm^{-1} can be indexed to the 100, 110, 200 and 210 reflections of an ordered 2D hexagonal (*p6mm*) mesostructure. The unit cell parameters of the as-prepared and calcined samples were 15.1 and 12.4 nm respectively, indicating a 17.9 % contraction of the titania network during calcination. From previous reports, SAXS results for calcined bulk 2D hexagonal meso-TiO_2 usually display only two or one peaks, although the corresponding patterns for as-synthesized samples distinctly show three peaks.[21-23] Additionally, the contraction ratio of hexagonal titania after calcination at 450 ºC here was relatively low in comparison to that found by others.[21, 24-25] Thus, this synthesis produced a very well-ordered stable meso-TiO_2 which exhibited only a small shrinkage upon calcination.

The TEM image in Figure 2 (right), shows a highly ordered degree of periodicity with a d-spacing of 10.6 nm, viewed from the (100) direction, further confirming the 2D hexagonal (*p6mm)* mesostructure suggested by SAXS. The diffraction pattern reveals the sample has a nanocrystalline structure and is in the anatase phase. The clear crystal rings in the inset diffraction pattern are attributed to the (101), (004), (200), (211) and (204) planes of the anatase phase, respectively.

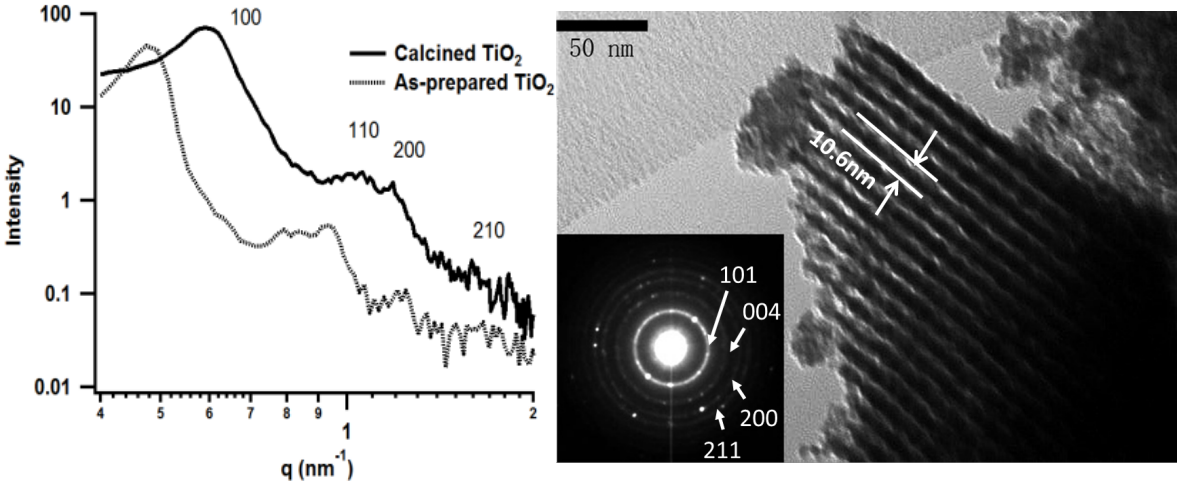

Figure 2 SAXS curves of as-prepared and calcined meso-TiO_2 (left); TEM image and diffraction pattern inset of calcined meso-TiO_2 (right).

The crystallographic structure of the calcined meso-TiO_2 powders was also confirmed by XRD analysis (Figure 3 (left)). All diffraction peaks can be unambiguously assigned to anatase TiO_2 (JCPDS card no. 21-1272), which is in agreement with the TEM diffraction pattern. Figure 3 (right) shows the nitrogen adsorption–desorption isotherms and pore size distribution of the meso-TiO_2. The isotherms can be classified as type IV with a pronounced H1 hysteresis loop and show a sharp capillary condensation step at a relative pressure of 0.7-0.9, suggesting a narrow pore size distribution and the existence of large mesopores with an open-ended cylindrical shape in this sample.[26-27] The pore-size distribution of samples was analysed by the Barrett−Joyner−Halenda (BJH) method. The predominant pore size is around 8.33 nm and they are uniform and narrowly distributed. To the best of our knowledge, such pore size is one of the largest reported for ordered mesoporous titania synthesized from the P123 template without any swelling agents.[28] The big pores improve the accessible pore volume, allowing improved adsorption of dye molecules on the internal surface.[29] The Brunauer−Emmett−Teller (BET) surface area of the meso-TiO_2 is 121 m^2/g.

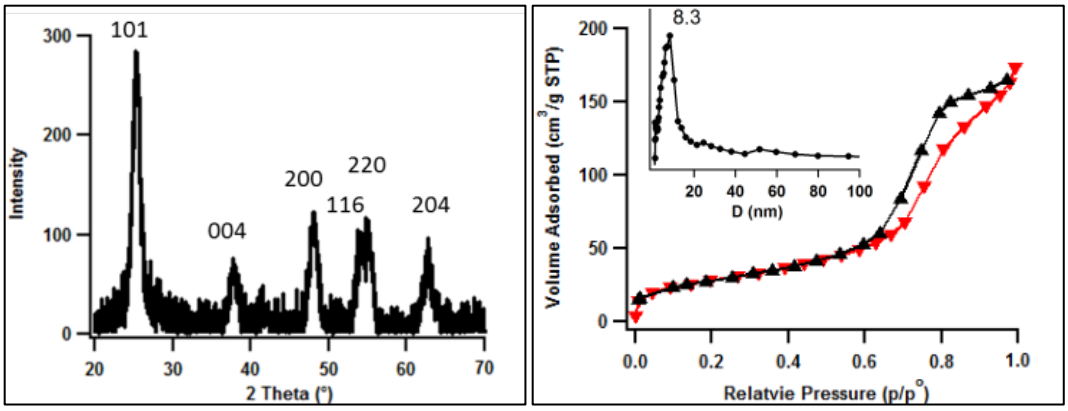

Figure 3 Wide-angle powder XRD curve (left) and N_2 ads/desorption isotherms (right) and pore size distribution of meso-TiO_2 (inset).

The properties of the meso-TiO_2/P25 composite films were also investigated by wide angle powder XRD (Figure 4). Only the anatase phase was found in the meso-100 sample, while the other films contained both anatase and rutile phases as small amount of the rutile phase is present in the P25 nanoparticles. According to the following equation [30]:

$$W_R = \frac{I_R}{0.886I_A + I_R}$$

the mass fraction of rutile (W_R) in the samples can be calculated by measuring the intensities of the strongest (110) and (101) diffraction peaks of rutile (I_R) and anatase (I_A), respectively. The results are listed in Table 1. It can be seen that the mass fraction of rutile phase decreases with increasing weight ratio of meso-TiO_2.

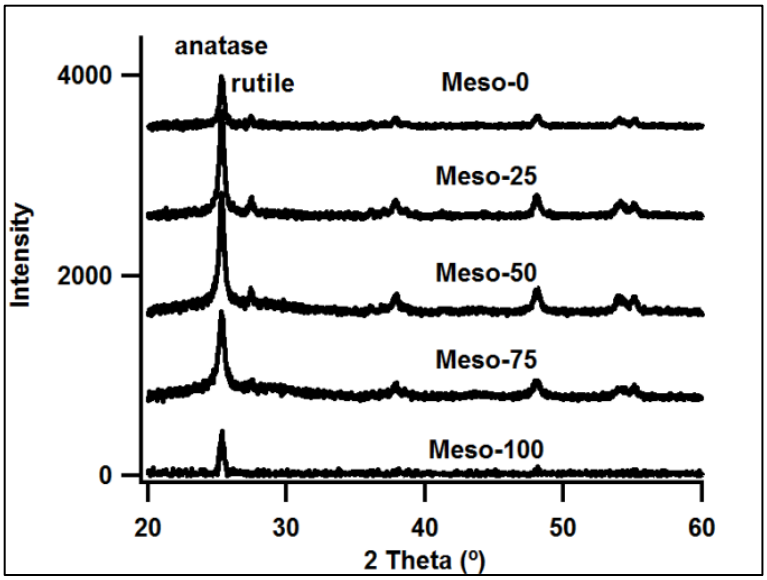

Figure 4 XRD curves of meso-X (X=0, 25, 50, 75 and 100).

Table 1. Textural properties of meso-TiO_2/P25 composite films.

Sample	Meso-0	Meso-25	Meso-50	Meso-75	Meso-100
Anatase and rutile phase ratio	80:20	85:15	90:10	95:5	100:0
RMS roughness (nm)	31	100	160	220	301
S_{BET} (m^2/g)	46±2	69±2	127±2	127±2	157±2
Pore volume (cm^3/g)	0.39±0.01	0.26±0.01	0.70±0.01	0.65±0.01	0.33±0.01
Adsorbed Dye ($nmol/cm^2$)	141±2	151±2	172±3	174±3	188±3

Figure 5 shows a SEM image of the top view of the films with inset cross-sectional images of meso-X (X=0, 25, 50, 75 and 100) films. SEM showed that films were homogenous on the micron-scale. With the increase in weight ratio of meso-TiO_2, the films became rougher as a result of the growing number of these larger titania particles. By adding meso-TiO_2, the films look more porous than the meso-0 film according to the magnified SEM surface images.

However, the meso-100 layer can be easily peeled off the ITO glass substrate after calcination, while others are more robust. This is because the films made entirely from meso-TiO_2 contained large aggregates with open space between them, leading to a weaker and less compact film. From the inset cross-sectional images, it can be seen that the first layer of the five photoelectrodes has exactly the same thickness (5 μm) and morphology, which should remove effects arising from the first layer when comparing the solar cell performance using different bilayer electrodes. The thickness of the meso-X films is around 5 μm and it is also easily seen that they have a smooth edge except in the case of the meso-100 film, due to its loosely compacted structure. AFM images of meso-X (X=0, 25, 50, 75 and 100) films were measured to further confirm the SEM results, and can be found in Figure S2 (supporting information). With the increase of weight ratio of meso-TiO_2, films became rougher with larger surface aggregates visible. The root mean square (RMS) roughness of the films is summarized in Table 1. The RMS roughness increased from 31 to 301 nm when the weight ratio of introduced meso-TiO_2 was varied from 0 to 100, which is in accordance with the SEM results.

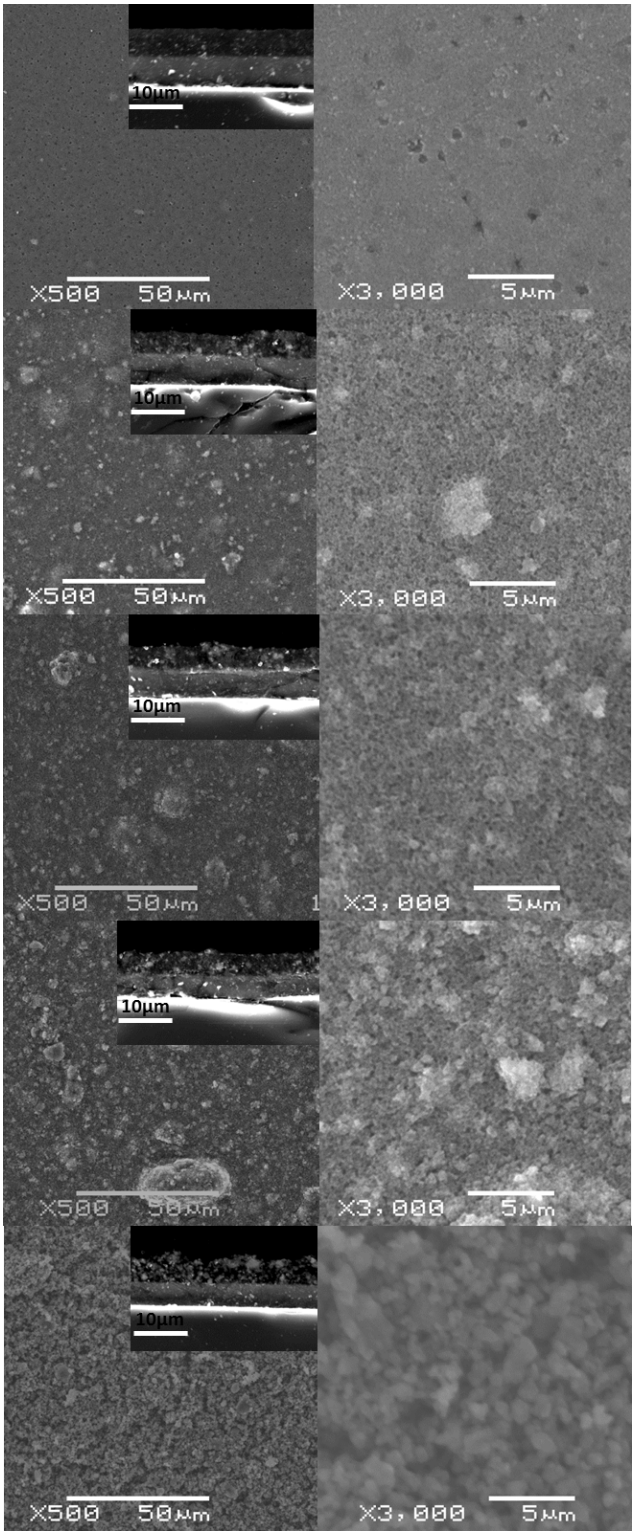

Figure 5 Top view with inset cross-sectional images of meso-X (X=0, 25, 50, 75 and 100) films from top to bottom by SEM. Left: low magnification, right: higher magnification.

Table 1 reports results from nitrogen adsorption–desorption isotherms and pore size distribution of meso-X (X=0, 25, 50, 75 and 100, see also Figure S3 in supporting information) As the meso-TiO_2 was already calcined at 450 ºC for 3 hrs prior to mixing with the P25 in pastes to form the films, the isotherms of meso-100 films look very similar to those of the meso-TiO_2 powder, although the pore size distribution is a little wider due to the collapse of pores during the grinding and ultrasonication processes of paste preparation. The BET surface area of the meso-100 film is 157 m^2/g, which is more than 3 times higher than that of the meso-0 films (46 m^2/g). After the introduction of P25 particles into the meso-TiO_2 film, the shape of the sorption isotherms changed and the hysteresis loop became smaller. The surface area decreased because P25 is a non-porous material and as a result has a much lower surface area than meso-TiO_2. The predominant internal pore size of meso-100 films is around 8.33 nm arising from the internal pores of meso-TiO_2, while the larger pores in P25 films arise from the space within nanoparticle aggregates and open space between aggregates.[16] No macropores were observed in meso-100 films because the open space between aggregates are too big to be analysed using BJH models.[31] The change in composition of the films caused variation in the pore size distribution and pore volumes in the films (Table 1). Obviously, the meso-100 film has the highest surface area but also the lowest pore volume due to the lack of macropores. Meso-50 and meso-75 films shared a very similar surface area but the meso-50 film had a higher pore volume. Considering the surface area and porosity, the optimum composite is likely to be the meso-50 film with a pore volume of 0.70 cm^3/g and surface area of 127 m^2/g.

Dye uptake into the composite films was measured and dye coverage is also listed in Table 1. The meso-100 photoelectrode contained the most dye, while the meso-0 film (100% P25) shows the lowest dye coverage. By adding the meso-TiO_2, more dye was absorbed by the films.

Scattering layers prepared from commercial paste or large particles normally have a low surface area < 30 m^2/g, [15, 32-34] but the meso-TiO_2/P25 composite films have a much higher surface area, which increases the dye loading.

To investigate the light scattering effects of the meso-X (X=0, 25, 50, 75 and 100) films for DSSC photoanodes, the reflectance spectra of the five photoanodes, shown in Figure 6 were compared. The meso-100 electrode had the highest reflectance, as it is composed of large secondary particulates with a strong light scattering effect, while the meso-0 film showed the lowest scattering due to the much smaller size of P25 particles. When adding the meso-TiO_2 into the nanoparticle film, the reflectance greatly improved due to the scattering effects of these large particles. The meso-50 film shares a similar value with that of the meso-75 film, despite the meso-75 film containing more large aggregated particles. This is because the meso-50 film had a higher number of macropores than the meso-75 film (refer to the BJH pore distribution in Figure S3) which could also serve as scattering centres.[35] The inset in Figure 6 shows the appearance of the meso-X photoanodes. For the meso-0 film, the words on the sheet beneath the photoanode can still be identified, whereas the words under other samples became gradually less clear as the weight ratio of meso-TiO_2 was increased, and are completely obscured by the meso-100 film because of the intense light scattering effect of the micrometre sized aggregates of meso-TiO_2. It is worth mentioning that the transparency of the meso-50 and meso-75 films is quite similar.

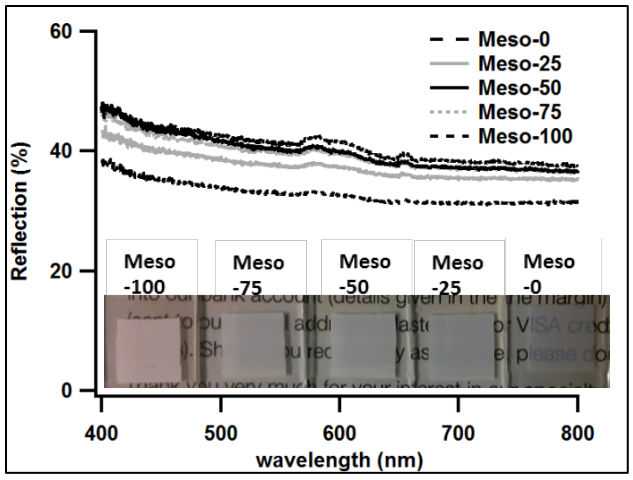

Figure 6 Reflection spectra and photographs of meso-X films.

Figure 7 shows the IV curves for DSSC prepared with meso-X. In total five sets of DSSC with the 5 different amounts of meso-TiO_2 were prepared, and typical results are shown here. Incorporation of the meso-TiO_2 increased the short current (J_{sc}) 10-15 %, while the fill factor (FF) was not appreciably changed. In contrast, the open circuit voltage (V_{oc}) was decreased slightly by 10–20 mV, possibly because the higher surface area of these films provides more recombination sites.[7, 36] It is also possible that some of the dye adsorbed within the mesopores is not easily accessible to the electrolyte, increasing geminate recombination with the dye.[37] IPCE curves are also shown in Figure 7. DSSC containing ≥ 25 % meso-TiO_2 showed a better photoelectrical response, with IPCEs that were higher than for the meso-0 cell over the entire wavelength range 400–800 nm. This is also in good agreement with the enhanced light scattering and dye adsorption as discussed above.

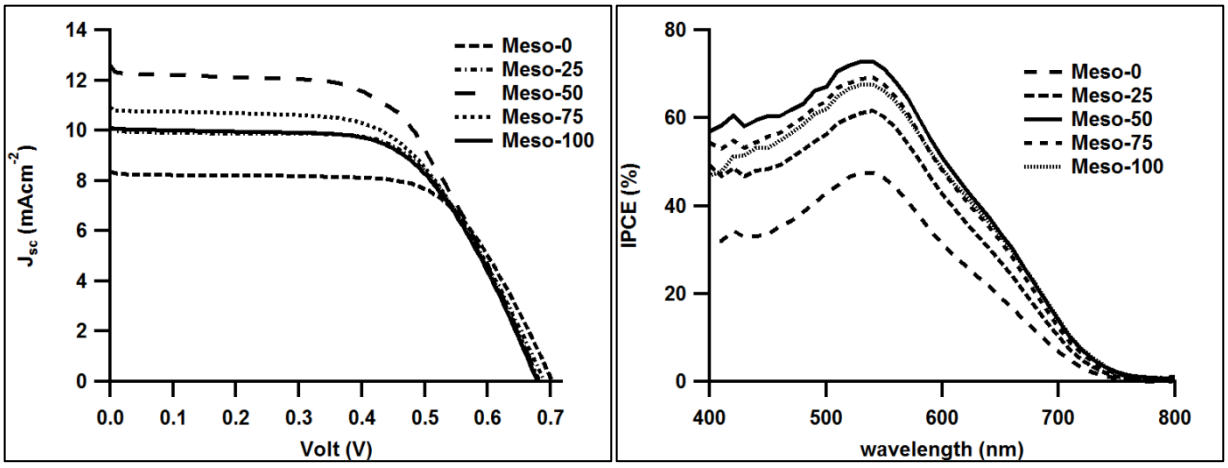

Figure 7 IV curves (left) and IPCE (right) of meso-X film DSSC.

Details of the photoelectrical properties are displayed in Table 2. The other four sets of meso-X solar cells share the same trend, however only one typical result was shown here. The efficiency found in our work is around 4-5 %, which is not as high as that reported in literature, [9-10, 15-16, 38] where other types of meso-TiO_2 secondary particles were applied in DSSC. However, the previous studies all used small area cells (0.16-0.36 cm^2) and had some post-treatment such as a $TiCl_4$ treatment which has been demonstrated to improve efficiency of DSSC. In this work, we focused on larger 1 cm^2 cells without any post-treatment to compare only the effects of using the meso-TiO_2 aggregates and P25 nanoparticles mixtures as the scattering layer. Larger test cells, as used here, typically result in lower efficiencies than are observed for very small area cells or those where extensive optimization has been carried out. Five cells for each meso-TiO_2-P25 mixture were prepared, so that reproducible trends in behavior could be ascertained. No further optimization of the cells was carried out since the purpose of the work was to study the influence of film structure, morphology, optical properties and cell performance to obtain a suitable combination of nanoparticles and scattering particles rather than to aim for high efficiency as an end goal in itself.

The total efficiency of the cells increased when meso-TiO_2 was added. The efficiency is expected to increase due to the presence of the scattering particles, however in this case the relative increase is greater as the mesoporous particles can themselves hold dye molecules. The observed increase in efficiency thus is due to both the increased surface area and hence increased dye loadings in the composite films as well as the increased light scattering. However, the meso-100 cell with the highest surface area and strongest scattering effects did not show the highest efficiency. This could be attributed to the fact that the meso-100 films had the highest dye loadings but a low porosity, suggesting that losses could be incurred due to poor infiltration of the electrolyte into the large aggregates.[39] In addition the meso-100 aggregates may not provide efficient electron transfer pathways for electron extraction. It is reasonable that the meso-25 cell has the second lowest efficiency out of the five cells, which results from its lower surface area and the smaller quantity of big particulates, which means lower dye loading and weaker scattering effects. The highest efficiency obtained for meso-50 might be attributed to the following facts: firstly, meso-50 films have the highest pore volume, which allows the electrolyte to penetrate into macropores and directly contact dye molecules. Secondly, it shows high dye loadings and strong scattering. It is interesting that the meso-75 cells showed a lower efficiency than meso-50 cells. Meso-75 cells show similar dye loading and scattering effects, and only slightly reduced porosity when compared to meso-50 cell. The issue may be the increase in the number of large aggregates in the meso-75 films, which do not provide good pathways for electron extraction.

Table 2. Photoelectric properties of meso-X film solar cells. The uncertainties in these values were calculated from the maximum difference from values for a total of 5 cells prepared in an identical manner.

Sample	Meso-0	Meso-25	Meso-50	Meso-75	Meso-100
J_{sc} (mA/cm^2)	8.36±0.01	9.82±0.01	11.96±0.01	10.26±0.01	9.32±0.01
V_{oc} (mV)	706±1	688±1	680±1	687±1	684±1
FF (%)	65±1	62±1	62±1	62±1	65±1
η (%)	3.85±0.26	4.26±0.29	4.93±0.32	4.38±0.36	4.21±0.38
IPCE at 530nm (%)	48±1	61±1	73±1	69±1	68±1

Conclusion

Highly ordered anatase 2D-hexagonal mesoporous titania powders with high surface area and large pores were synthesized. The introduction of meso-TiO_2 into P25 titania films, caused the films to become more porous, rougher and have higher surface area. Moreover, aggregates of meso-TiO_2 in films increases the amount of light scattering. Most importantly the amount of dye that could be adsorbed onto the photoanode increased with the fraction of meso-TiO_2. These contributed to an improvement of the photovoltaic performances when meso-TiO_2 was added to a P25 layer in DSSCs. Although the meso-100 cell has some superior properties such as surface area and scattering effects, it did not show the best cell performance mainly due to the poor connectivity of micron-sized meso-TiO_2 aggregates that increase the electron diffusion

resistance. Considering the porosity, surface area, scattering effects and the degree of compactness of the film, the optimum cell was obtained by introducing 50 wt.% meso-TiO_2, which shows an increase of short current from 8.36 to 11.96 mA/cm^2 and an increase in efficiency from 3.85 to 4.93 % compared to an equivalent cell prepared with the P25 film.

AUTHOR INFORMATION

Corresponding Author

*Department of Chemistry, University of Bath, Claverton Down, Bath BA2 7AY, UK. Fax: 44 1225 386231; Tel: 44 1225 384192; E-mail: K.edler@bath.ac.uk

ACKNOWLEDGMENT

This work was supported by an Overseas Student Scholarship from University of Bath and a scholarship from the China Scholarship Council. We also acknowledge the help of Thomas Risbridger in the fabrication of solar cells and of John Mitchels for SEM measurements.

Supporting Information. Thermogravimetric measurement on as-synthesised meso-TiO_2, AFM images of Meso-X (X=0, 25, 50, 75 and 100) films, N_2 sorption isotherms of meso-X films and pore size distributions calculated using the BJH method. This material can be found online and free of charge at http://pubs.acs.org.

REFERENCES

1. Yella, A.; Lee, H.-W.; Tsao, H. N.; Yi, C.; Chandiran, A. K.; Nazeeruddin, M. K.; Diau, E. W.-G.; Yeh, C.-Y.; Zakeeruddin, S. M.; Grätzel, M., Porphyrin-Sensitized Solar Cells with Cobalt (Ii/Iii)–Based Redox Electrolyte Exceed 12 Percent Efficiency. *Science* **2011**, *334*, 629-634.
2. Markvart, T., *Solar Electricity*; John Wiley & Sons, 2000.
3. Hagfeldt, A.; Boschloo, G.; Sun, L. C.; Kloo, L.; Pettersson, H., Dye-Sensitized Solar Cells. *Chemical Reviews* **2010**, *110*, 6595-6663.
4. Zhang, Q. F.; Cao, G. Z., Nanostructured Photoelectrodes for Dye-Sensitized Solar Cells. *Nano Today* **2011**, *6*, 91-109.
5. Deepak, T. G.; Anjusree, G. S.; Thomas, S.; Arun, T. A.; Nair, S. V.; Sreekumaran Nair, A., A Review on Materials for Light Scattering in Dye-Sensitized Solar Cells. *RSC Advances* **2014**, *4*, 17615-17638.
6. Koo, H.-J.; Park, J.; Yoo, B.; Yoo, K.; Kim, K.; Park, N.-G., Size-Dependent Scattering Efficiency in Dye-Sensitized Solar Cell. *Inorganica Chimica Acta* **2008**, *361*, 677-683.
7. Yu, I. G.; Kim, Y. J.; Kim, H. J.; Lee, C.; Lee, W. I., Size-Dependent Light-Scattering Effects of Nanoporous Tio2 Spheres in Dye-Sensitized Solar Cells. *J. Mater. Chem.* **2010**, *21*, 532-538.
8. Wang, Z.-S.; Kawauchi, H.; Kashima, T.; Arakawa, H., Significant Influence of Tio2 Photoelectrode Morphology on the Energy Conversion Efficiency of N719 Dye-Sensitized Solar Cell. *Coordination Chemistry Reviews* **2004**, *248*, 1381-1389.
9. Cheng, W.-Y.; Deka, J. R.; Chiang, Y.-C.; Rogeau, A.; Lu, S.-Y., One-Step, Surfactant-Free Hydrothermal Method for Syntheses of Mesoporous Tio2 Nanoparticle Aggregates and Their Applications in High Efficiency Dye-Sensitized Solar Cells. *Chemistry of Materials* **2012**, *24*, 3255-3262.
10. Gajjela, S. R.; Yap, C.; Balaya, P., Multi-Functional Photoanode Films Using Mesoporous Tio2 Aggregate Structure for Efficient Dye Sensitized Solar Cells. *Journal of Materials Chemistry* **2012**, *22*, 10873-10882.
11. Chen, D.; Huang, F.; Cheng, Y.-B.; Caruso, R. A., Mesoporous Anatase Tio2 Beads with High Surface Areas and Controllable Pore Sizes: A Superior Candidate for High-Performance Dye-Sensitized Solar Cells. *Advanced Materials* **2009**, *21*, 2206-2210.
12. Sauvage, F.; Chen, D.; Comte, P.; Huang, F.; Heiniger, L.-P.; Cheng, Y.-B.; Caruso, R. A.; Graetzel, M., Dye-Sensitized Solar Cells Employing a Single Film of Mesoporous Tio2 Beads Achieve Power Conversion Efficiencies over 10%. *ACS Nano* **2010**, *4*, 4420-4425.
13. Zhang, H.; Han, Y.; Liu, X.; Liu, P.; Yu, H.; Zhang, S.; Yao, X.; Zhao, H., Anatase Tio2 Microspheres with Exposed Mirror-Like Plane {001} Facets for High Performance Dye-Sensitized Solar Cells (Dsscs). *Chemical Communications* **2010**, *46*, 8395-8397.
14. Gao, Z.; Wu, Z.; Li, X.; Chang, J.; Wu, D.; Ma, P.; Xu, F.; Gao, S.; Jiang, K., Application of Hierarchical Tio2 Spheres as Scattering Layer for Enhanced Photovoltaic Performance in Dye Sensitized Solar Cell. *CrystEngComm* **2013**, *15*, 3351-3358.
15. Han, S.-H.; Lee, S.; Shin, H.; Suk Jung, H., A Quasi-Inverse Opal Layer Based on Highly Crystalline Tio2 Nanoparticles: A New Light-Scattering Layer in Dye-Sensitized Solar Cells. *Advanced Energy Materials* **2011**, *1*, 546-550.

16. Kim, Y. J.; Lee, M. H.; Kim, H. J.; Lim, G.; Choi, Y. S.; Park, N.-G.; Kim, K.; Lee, W. I., Formation of Highly Efficient Dye-Sensitized Solar Cells by Hierarchical Pore Generation with Nanoporous Tio2 Spheres. *Advanced Materials* **2009**, *21*, 3668-3673.
17. Zhang, R.; Tu, B.; Zhao, D., Synthesis of Highly Stable and Crystalline Mesoporous Anatase by Using a Simple Surfactant Sulfuric Acid Carbonization Method. *Chemistry – A European Journal* **2010**, *16*, 9977-9981.
18. Lee, Y.-F.; Chang, K.-H.; Hu, C.-C.; Lin, K.-M., Synthesis of Activated Carbon-Surrounded and Carbon-Doped Anatase Tio2 Nanocomposites. *Journal of Materials Chemistry* **2010**, *20*, 5682-5688.
19. Smarsly, B.; Grosso, D.; Brezesinski, T.; Pinna, N.; Boissière, C.; Antonietti, M.; Sanchez, C., Highly Crystalline Cubic Mesoporous Tio2 with 10-Nm Pore Diameter Made with a New Block Copolymer Template. *Chemistry of Materials* **2004**, *16*, 2948-2952.
20. Narayan, K.; Anderson, M. T.; Brinker, C. J., Template-Based Approaches to the Preparation of Amorphous, Nanoporous Silicas. *Chemistry of Materials* **1996**, *8*, 1682-1701.
21. Choi, S. Y.; Mamak, M.; Coombs, N.; Chopra, N.; Ozin, G. A., Thermally Stable Two-Dimensional Hexagonal Mesoporous Nanocrystalline Anatase, Meso-Nc-Tio2: Bulk and Crack-Free Thin Film Morphologies. *Advanced Functional Materials* **2004**, *14*, 335-344.
22. Mohd Ibrahim, S.; Masrom, A.; Mazinani, B.; Radiman, S.; Md Jamil, F.; Beitollahi, A.; Negishi, N.; Yahya, N., Mesoporous Titania Photocatalyst: Effect of Relative Humidity and Aging on the Preparation of Mesoporous Titania and on Its Photocatalytic Activity Performance. *Res Chem Intermed* **2013**, *39*, 1003-1014.
23. Guldin, S., et al., Improved Conductivity in Dye-Sensitised Solar Cells through Block-Copolymer Confined Tio2 Crystallisation. *Energy & Environmental Science* **2011**, *4*, 225-233.
24. Zhou, H.; Wang, C.; Feng, Z.; Li, S.; Xu, B., Formation of Grid-Like Mesoporous Titania Film Via Structural Transformation and Its Surface Superhydrophilicity Conversion. *Surface and Coatings Technology* **2012**, *207*, 34-41.
25. Lee, J.; Orilall, M.; Warren, S.; Kamperman, M.; DiSalvo, F.; Wiesner, U., Direct Access to Thermally Stable and Highly Crystalline Mesoporous Transition-Metal Oxides with Uniform Pores. *Nature Materials* **2008**, *7*, 222-228.
26. Horikawa, T.; Do, D. D.; Nicholson, D., Capillary Condensation of Adsorbates in Porous Materials. *Advances in Colloid and Interface Science* **2011**, *169*, 40-58.
27. Liu, J.; An, T.; Li, G.; Bao, N.; Sheng, G.; Fu, J., Preparation and Characterization of Highly Active Mesoporous Tio2 Photocatalysts by Hydrothermal Synthesis under Weak Acid Conditions. *Microporous and Mesoporous Materials* **2009**, *124*, 197-203.
28. Liu, K.; Fu, H.; Shi, K.; Xiao, F.; Jing, L.; Xin, B., Preparation of Large-Pore Mesoporous Nanocrystalline Tio2 Thin Films with Tailored Pore Diameters. *The Journal of Physical Chemistry B* **2005**, *109*, 18719-18722.
29. Yun, T. K.; Park, S. S.; Kim, D.; Hwang, Y.-K.; Huh, S.; Bae, J. Y.; Won, Y. S., Pore-Size Effect on Photovoltaic Performance of Dye-Sensitized Solar Cells Composed of Mesoporous Anatase-Titania. *Journal of Power Sources* **2011**, *196*, 3678-3682.
30. Zhou, M.; Yu, J.; Liu, S.; Zhai, P.; Jiang, L., Effects of Calcination Temperatures on Photocatalytic Activity of Sno2/Tio2 Composite Films Prepared by an Epd Method. *Journal of Hazardous Materials* **2008**, *154*, 1141-1148.
31. Barrett, E. P.; Joyner, L. G.; Halenda, P. P., The Determination of Pore Volume and Area Distributions in Porous Substances. I. Computations from Nitrogen Isotherms. *Journal of the American Chemical society* **1951**, *73*, 373-380.

32. Ohno, T.; Sarukawa, K.; Matsumura, M., Photocatalytic Activities of Pure Rutile Particles Isolated from Tio2 Powder by Dissolving the Anatase Component in Hf Solution. *The Journal of Physical Chemistry B* **2001**, *105*, 2417-2420.
33. Barringer, E. A.; Bowen, H. K., High-Purity, Monodisperse Tio2 Powders by Hydrolysis of Titanium Tetraethoxide. 1. Synthesis and Physical Properties. *Langmuir* **1985**, *1*, 414-420.
34. Almquist, C. B.; Biswas, P., Role of Synthesis Method and Particle Size of Nanostructured Tio2 on Its Photoactivity. *Journal of Catalysis* **2002**, *212*, 145-156.
35. Gao, X.-D.; Li, X.-M.; Gan, X.-Y.; Wu, Y.-Q.; Zheng, R.-K.; Wang, C.-L.; Gu, Z.-Y.; He, P., Aerogel Based Sio2-Tio2 Hybrid Photoanodes for Enhanced Light Harvesting in Dye-Sensitized Solar Cells. *Journal of Materials Chemistry* **2012**, *22*, 18930-18938.
36. Wu, W.-Q.; Lei, B.-X.; Rao, H.-S.; Xu, Y.-F.; Wang, Y.-F.; Su, C.-Y.; Kuang, D.-B., Hydrothermal Fabrication of Hierarchically Anatase Tio2 Nanowire Arrays on Fto Glass for Dye-Sensitized Solar Cells. *Scientific Reports* **2013**, *3*, 1352.
37. Ning, Z.; Fu, Y.; Tian, H., Improvement of Dye-Sensitized Solar Cells: What We Know and What We Need to Know. *Energy & Environmental Science* **2010**, *3*, 1170-1181.
38. Agarwala, S.; Kevin, M.; Wong, A. S. W.; Peh, C. K. N.; Thavasi, V.; Ho, G. W., Mesophase Ordering of Tio2 Film with High Surface Area and Strong Light Harvesting for Dye-Sensitized Solar Cell. *ACS Applied Materials & Interfaces* **2010**, *2*, 1844-1850.
39. van de Lagemaat, J.; Benkstein, K. D.; Frank, A. J., Relation between Particle Coordination Number and Porosity in Nanoparticle Films: Implications to Dye-Sensitized Solar Cells. *The Journal of Physical Chemistry B* **2001**, *105*, 12433-12436.

Table of Contents Graphic